2D Shallow Water Equations by Composite Schemes

Richard Liska[1], Burton Wendroff[2]
[1]*Faculty of Nuclear Sciences and Physical Engineering*
Czech Technical University in Prague
Břehová 7, 115 19 Prague 1, Czech Republic
(liska@siduri.fjfi.cvut.cz, http://www-troja.fjfi.cvut.cz/~liska)
[2]*Group T-7, Los Alamos National Laboratory*
Los Alamos, NM 87544, USA
(bbw@lanl.gov, http://math.unm.edu/~bbw)

November 25, 1997

Abstract

Composite schemes are formed by global composition of several Lax-Wendroff steps followed by a diffusive Lax-Friedrichs or WENO step which filters out the oscillations around shocks typical for the Lax-Wendroff scheme. These schemes are applied to the shallow water equations in 2D. The Lax-Friedrichs composite is also formulated for a trapezoidal mesh, which is necessary in several example problems. The suitability of the composite schemes for the shallow water equations is demonstrated on several examples including the circular dam break problem, the shock focussing problem and supercritical channel flow problems.

1 Introduction

The shallow water equations are a system of conservation laws. There are two simple well-known finite difference schemes for conservation laws, Lax-Wendroff (LW) and Lax-Friedrichs (LF). Both of these methods have some drawbacks. The LW scheme is second order accurate but oscillatory close to shocks. The LF scheme is non-oscillatory but also excessively diffusive. Composite schemes combine these two methods in an attempt to remove their deficiencies. One example of a composite scheme is a global composition of several LW steps followed by one diffusive LF step which serves as a consistent filter removing the unwanted oscillations. This simple construction is efficient and produces surprisingly good results. For more details see [1]. Another composite uses a component-wise formulation of WENO for the diffusive step. Here we apply these composite schemes to the shallow water equations in 2D.

The 2D shallow water equations have attracted quite a lot of attention in recent years. Alcrudo and Garcia-Navarro [2] developed a high-resolution Godunov-type MUSCL finite volume scheme. Glaister [3] used a flux splitting technique. Nadiga [4] designed an adaptive discrete-velocity model of the shallow water equations. Nadiga, Margolin and Smolarkiewicz [5] employed a semi-Lagrangian scheme on a massively parallel computer. Zienkiewicz and Ortiz [6] introduced a split-characteristic finite element method. Ambrosi [7] used Roe's Riemann solver with MUSCL slope limiting. Bova and Carey [8] developed a streamline upwind Petrov-Galerkin scheme. Morel, Fey and Maurer [9] decompose the shallow water equations into many advection equations which are then solved by a finite volume scheme with a special limiter. Lyra and Morgan used Galerkin-LED and MUSCL schemes on an adaptive unstructured mesh. More recently in 1997 Walters and Barragy [10] compared H and P finite element methods. Anastasiou [11] and Chan used a Godunov-type second order upwind finite volume method on unstructured triangular meshes. Chippada, Dawson, Martines and Wheeler [12] developed a Godunov-type finite volume method using Roe's approximation for solving the Riemann problems. Apparently there are many numerical methods for solving the shallow water equations. In this paper we apply composite schemes to solve this problem and show that they work remarkably well.

The paper is organized as follows. In section 2 we illustrate how composite schemes work for the shallow water equations in 1D. Section 3 presents the shallow water equations in 2D and the boundary conditions used. Section 4 covers the finite difference schemes on uniform rectangular meshes. In section 5 the finite difference schemes are newly developed on trapezoidal meshes which are needed for channel flow problems. Section 6 includes several numerical test problems demonstrating the usefulness of the composite schemes for the shallow water equations.

2 1D Illustration

The shallow water equations [13] in one dimension are

$$\begin{aligned} h_t + (hu)_x &= 0 \\ (hu)_t + \left(hu^2 + g\frac{1}{2}h^2\right)_x + ghz_{0x} &= 0. \end{aligned}$$

Here $h(x,t)$ is the thickness of the water layer, $u(x,t)$ is the velocity of the layer, $z_0(x)$ is the height of the bottom profile and g is the gravitational constant. We use here the bottom profile

$$z_0(x) = \begin{cases} b_c\left(1 - \frac{x^2}{4}\right) & \text{for } -2 \le x \le 2 \\ 0 & \text{otherwise.} \end{cases}$$

The initial conditions $h(x,0) + z_0(x) = 1, u(x,0) = u_0$ set the height of the water surface and the initial velocity to be constant. Free boundary conditions are applied.

For a system of conservation laws

$$U_t = f_x(U)$$

the two-step Lax-Friedrichs (LF) scheme defines new values on a staggered dual grid as

$$U_{i+1/2}^{n+1/2} = \frac{1}{2}[U_i^n + U_{i+1}^n] + \frac{\Delta t}{2\Delta x}[f(U_{i+1}^n) - f(U_i^n)], \tag{1}$$

and the solution on the original grid is obtained by the same formula shifted by 1/2 in the index i. The two-step Lax-Wendroff (LW) scheme uses the same predictor (1) for the first half step. In the second half step however it advances from the time level n to the time level $n+1$ using the fluxes from the time level $n+1/2$,

$$U_i^{n+1} = U_i^n + \frac{\Delta t}{\Delta x}[f(U_{i+1/2}^{n+1/2}) - f(U_{i-1/2}^{n+1/2})]. \tag{2}$$

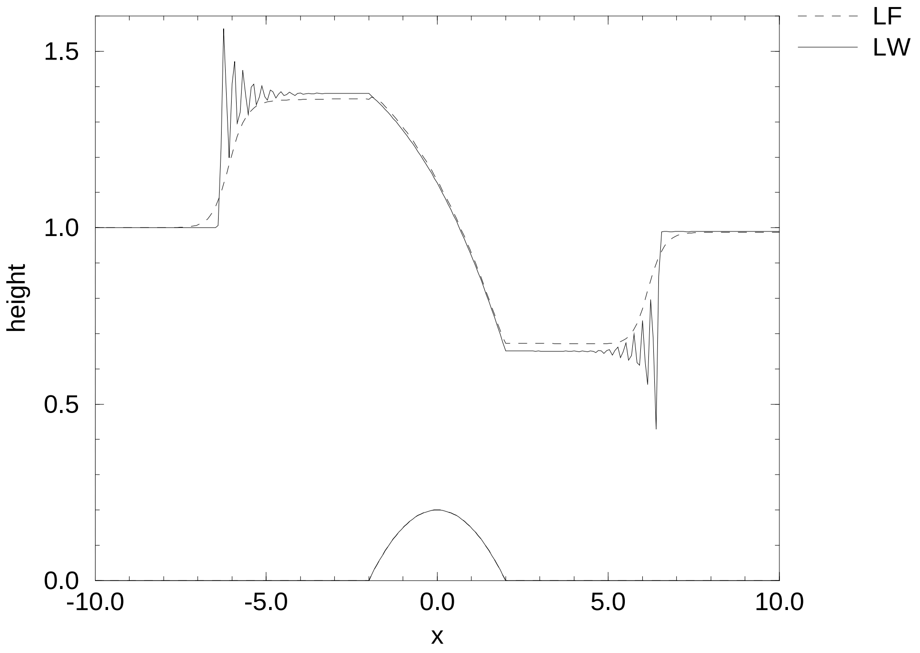

Figure 1: Heights of a 1D shallow water flow calculated by Lax-Friedrichs and Lax-Wendroff schemes.

It is well known that the LW scheme produces oscillations behind shocks while LF is excessively diffusive, smearing out the shocks. Both these phenomena are evident in Fig. 1, where the heights at $t = 20$ of the 1D shallow water flow over topography calculated by LF and LW schemes with 250 points is presented. In this problem we used $b_c = 0.2$, $u_0 = 1, g = 1$ and solved it in $x \in (-10, 10)$.

The composite scheme is defined by global composition of several LW steps followed by one LF step. We denote by L_W the operator defined by the LW scheme (1),(2) and by L_F the operator defined by the LF scheme (1), with both operators doing one time step from time level n to $n+1$. The difference operator S_k defined by $k-1$ applications of L_W followed by one application of L_F

$$S_k = L_F \circ L_W \circ \cdots \circ L_W, \tag{3}$$

then defines the composite scheme which we call LWLFk. The operator S_k operates from time level n to $n+k$, $U^{n+k} = S_k U^n$. The results of the same problem done by the composite LWLF4 scheme with 250 and 2000 points presented in Fig. 2 shows that the composite scheme eliminates the drawbacks of both LW and LF schemes. The solution is not oscillatory and the shock heights and speeds are resolved well. The solution with 2000 points should be a good approximation of the exact solution.

The LW scheme is second order while LF is only first order accurate which implies that the composite scheme is also only first order, however with a smaller coefficient of the leading error term. For more details of composite schemes, examples with 2D gas dynamics Riemann problems and tests with a second order diffusive WENO scheme instead of LF see [1].

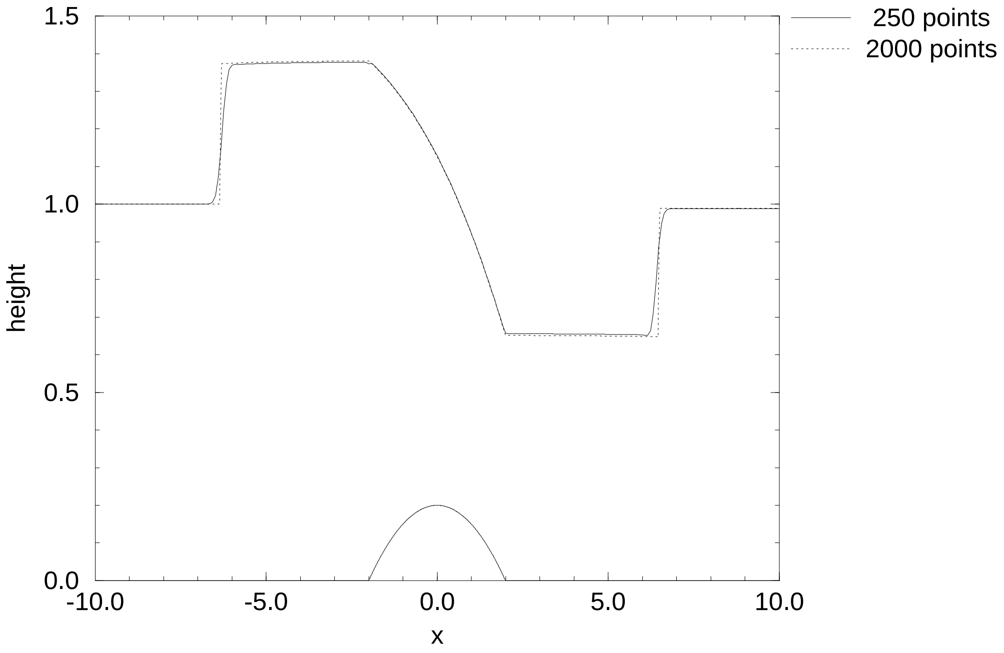

Figure 2: Heights of a 1D shallow water flow calculated by the composite LWLF4 scheme with 250 and 2000 points.

3 2D Shallow Water Equations

The shallow water system in 2D is described by the fluid layer thickness $h(t,x,y)$, x and y components of layer velocity $u(t,x,y), v(t,x,y)$. The shallow water equations are derived from 3D Euler equations by vertical averaging using hydrostatic pressure assumption. For numerical solution we use the conservative form of shallow water equations for conserved momenta hu, hv in the form

$$\begin{aligned} h_t + (hu)_x + (hv)_y &= 0 \\ (hu)_t + \left(hu^2 + \frac{1}{2}gh^2\right)_x + (huv)_y &= 0 \\ (hv)_t + (huv)_x + \left(hv^2 + \frac{1}{2}gh^2\right)_y &= 0, \end{aligned} \tag{4}$$

where g is gravitation constant. The x and y flux Jacobian matrices of the system are

$$\mathbf{A} = \begin{pmatrix} 0 & 1 & 0 \\ gh - u^2 & 2u & 0 \\ -uv & v & u \end{pmatrix}, \quad \mathbf{B} = \begin{pmatrix} 0 & 0 & 1 \\ -uv & v & u \\ gh - v^2 & 0 & 2v \end{pmatrix},$$

with eigenvalues $\{u, u \pm \sqrt{gh}\}$, and $\{v, v \pm \sqrt{gh}\}$, respectively.

On the inflow boundary we use fixed boundary conditions fixing the values of h, u, v on the boundary to a given value. On the free boundaries we use free boundary conditions, setting $h_n = 0, u_n = 0, v_n = 0$ where the subscript n denotes the derivative normal to the boundary. On the wall boundaries we use free slip boundary conditions, setting $h_n = 0$, and the velocity component normal to the boundary is set to zero.

4 Finite Difference Schemes on Uniform Rectangular Mesh

A uniform rectangular mesh is given by the points (x_i, y_j) with constant grid steps $\Delta x = x_{i+1} - x_i, \Delta y = y_{j+1} - y_j$. The dual mesh is given by the pints $(x_{i+1/2}, y_{j+1/2}) = (x_i + \Delta x/2, y_j + \Delta y/2)$. The basic idea of the new version of 2D Lax-Friedrichs, which is derived in [1], is based on the observation of Boukadida and LeRoux [14] that in order to implement a two-dimensional Godunov method to get cell averages on the dual grid from the averages on the primary grid one need only solve one-dimensional Riemann problems on the edges of the dual grid. The first half step of the new LF is, for the system of conservation laws in 2D

$$U_t = f_x(U) + g_y(U), \tag{5}$$

given by

$$\begin{aligned} U^{n+1/2}_{i+1/2,j+1/2} &= \frac{1}{4}[U^n_{i,j} + U^n_{i+1,j} + U^n_{i,j+1} + U^n_{i+1,j+1}] \\ &\quad + \frac{\Delta t}{2\Delta x}[F_{i+1,j+1/2} - F_{i,j+1/2}] + \frac{\Delta t}{2\Delta y}[G_{i+1/2,j+1} - G_{i+1/2,j}], \end{aligned} \tag{6}$$

where the fluxes F, G are evaluated at the LF approximate solution of the 1D Riemann problems at time level $n + 1/4$, giving

$$F_{i+1,j+1/2} = f\left(\frac{1}{2}[U^n_{i+1,j+1} + U^n_{i+1,j}] + \frac{\Delta t}{4\Delta y}[g(U^n_{i+1,j+1}) - g(U^n_{i+1,j})]\right), \tag{7}$$

and

$$G_{i+1/2,j+1} = g\left(\frac{1}{2}[U^n_{i+1,j+1} + U^n_{i,j+1}] + \frac{\Delta t}{4\Delta x}[f(U^n_{i+1,j+1}) - f(U^n_{i,j+1})]\right). \tag{8}$$

The second half step of the LF scheme going from the dual to the primary mesh is given by the same fomulas shifted by $1/2$ in the indices i, j.

The corresponding second order accurate predictor-corrector scheme, which we call corrected Lax-Friedrichs (CF), is then

$$\begin{aligned} U^{n+1}_{i,j} &= U^n_{i,j} \\ &+ \frac{\Delta t}{2\Delta x}[f(U^{n+1/2}_{i+1/2,j+1/2}) + f(U^{n+1/2}_{i+1/2,j-1/2}) - f(U^{n+1/2}_{i-1/2,j+1/2}) - f(U^{n+1/2}_{i-1/2,j-1/2})] \\ &+ \frac{\Delta t}{2\Delta y}[g(U^{n+1/2}_{i+1/2,j+1/2}) + g(U^{n+1/2}_{i-1/2,j+1/2}) - g(U^{n+1/2}_{i+1/2,j-1/2}) - g(U^{n+1/2}_{i-1/2,j-1/2})] \end{aligned}$$

where the predictor half-step is defined by the LF half step (6). One could thought about averaging $U^{n+1/2}$ before applying f or g. We have tried this idea however it does not work well for the shock focusing example from the section 6.2.

The composite schemes are constructed by the same way as in 1D (3) and are denoted by CFLFk. For more details see [1] where we have shown that both the LF and CF schemes are optimally stable for the scalar advection equation (5) with $f = aU, g = bU$, i.e. their stability condition is $\max(|a\Delta t/\Delta x|, |b\Delta t/\Delta x|) \leq 1$, which is also the stability condition of the composite schemes in that case. No stability analysis is available for systems, but our computations indicate that the composite schemes for shallow water are stable with the condition

$$\max(|u \pm \sqrt{gh}|\Delta t/\Delta x, |v \pm \sqrt{gh}|\Delta t/\Delta x) \leq 1.$$

The time interval Δt is adaptively determined from this stability condition after each time step.

In [1] we have also experimented with a second order diffusive WENO [15] scheme replacing the LF step in the composite schemes. We do not use the eigenvector decomposition as in [15] and apply the WENO procedure directly to the conserved variables. We call such scheme component-wise WENO (CW) and the composite is then CFCWk. We give one numerical test of this composite later.

5 Trapezoidal Mesh

For the supercritical channel flow problems described in the section 6.3 we need to solve the shallow water equations on a mesh with trapezoidal cells. Here we develop the Lax-Friedrichs (LF) and corrected Friedrichs (CF) finite difference schemes on trapezoidal meshes.

Both schemes use the standard device of approximating $f_x + g_y$ in a convex polygonal cell with area A by

$$f_x + g_y \equiv \frac{1}{A} \int \int (f_x + g_y) dx dy \equiv \frac{1}{A} \oint -f dy + g dx, \tag{9}$$

with the line integral taken counterclockwise. The integrals of f and g along the edges are then approximated by some form of midpoint or trapezoidal rule.

5.1 Mesh

The solution region is a trapezoid defined by four corners $[(x_a, y_a), (x_b, y_b), (x_a, y_c), (x_b, y_d)]$. The grid indices (i, j) correspond to (x, y) coordinates. The grid has (n_i, n_j) points in (x, y) directions. The mesh is uniform in the x coordinate.

$$\Delta x = \frac{x_b - x_a}{n_i - 1}, \qquad x_i = x_a + (i-1)\Delta x$$

The trapezoidal mesh is constructed so that the grid intervals in y depend only on the x index i, i.e. the y grid step on each grid line parallel to the y coordinate axis is constant.

$$\Delta y_i = y_{i,j+1} - y_{i,j} = \Delta y_1 + (i-1) \frac{\Delta y_{n_1} - \Delta y_1}{n_i - 1},$$

where the first and last grid steps are given by

$$\Delta y_1 = \frac{y_c - y_a}{n_j - 1}, \qquad \Delta y_{n_i} = \frac{y_d - y_b}{n_j - 1}.$$

The y coordinates of the node (i, j) are

$$y_{i,j} = y_a + (i-1) \frac{y_b - y_a}{n_i - 1} + (j-1)\Delta y_i.$$

The y coordinates of the dual staggered grid are

$$y_{i+1/2,j+1/2} = \frac{1}{4} \left(y_{i,j} + y_{i+1,j} + y_{i+1,j+1} + y_{i,j+1} \right).$$

The area of the cell $(i+1/2, j+1/2)$, i.e. of the trapezoid with corners at nodes $[(i,j),(i+1,j),(i+1,j+1),(i,j+1)]$, is

$$S_i = \frac{\Delta y_i + \Delta y_{i+1}}{2}\Delta x.$$

The area of the trapezoid with corners $[(i,j),(i+1/2,j),(i+1/2,j+1/2),(i,j+1/2)]$ is

$$s_i = \frac{3\Delta y_i + \Delta y_{i+1}}{16}\Delta x$$

and the area of the trapezoid with corners $[(i+1/2,j),(i+1,j),(i+1,j+1/2),(i+1/2,j+1/2)]$ is

$$s_{i+1/2} = \frac{\Delta y_i + 3\Delta y_{i+1}}{16}\Delta x.$$

5.2 LF Predictor

A part of the primary grid which is used in the construction of LF predictor scheme is shown in Fig. 3.

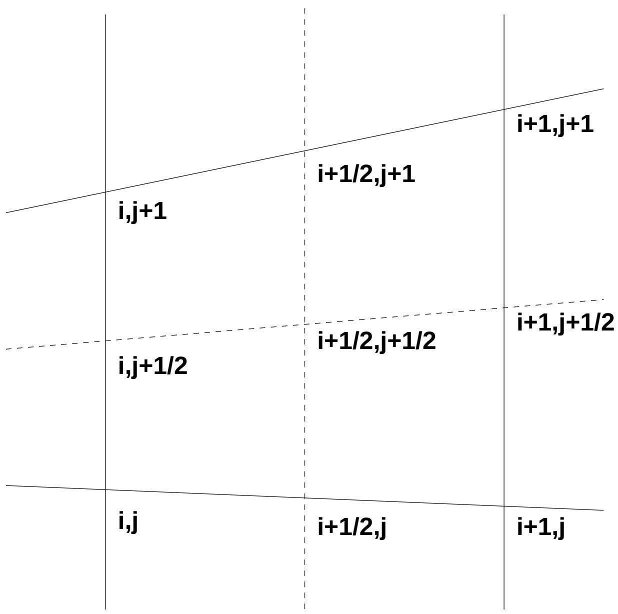

Figure 3: A part of the primary grid used in the LF predictor

The LF predictor operates from the node values on the original grid at the time level n to the dual staggered grid at the time level $n+1/2$, using the staggered Godunov idea of [14] and also (9). For our special trapezoids the difference equations are

$$\begin{aligned}
S_i U^{n+1/2}_{i+1/2,j+1/2} &= s_i U^n_{i,j} + s_{i+1/2} U^n_{i+1,j} + s_{i+1/2} U^n_{i+1,j+1} + s_i U^n_{i,j+1} \\
&\quad - \frac{\Delta t}{2}\Big[-F_{i+1/2,j}(y_{i+1,j} - y_{i,j}) - F_{i+1,j+1/2}(y_{i+1,j+1} - y_{i+1,j}) \\
&\qquad + F_{i+1/2,j+1}(y_{i+1,j+1} - y_{i,j+1}) + F_{i,j+1/2}(y_{i,j+1} - y_{i,j})\Big] \\
&\quad + \frac{\Delta t \Delta x}{2}\Big[G_{i+1/2,j+1} - G_{i+1/2,j}\Big],
\end{aligned} \tag{10}$$

where the fluxes F, G are given by

$$F_{kl} = f(U_{kl}^{n+1/4}), G_{kl} = g(U_{kl}^{n+1/4}),$$

with $U^{n+1/4}$ denoting the approximate solution of an appropriate 1D Riemann problem. For the horizontally oriented edges this is a Riemann problem in a rotated coordinate system, and the LF approximation is

$$U_{i+1/2,j}^{n+1/4} = \frac{1}{2}\left(U_{i,j}^n + U_{i+1,j}^n\right) + \frac{\Delta t}{4}\frac{(f(U_{i+1,j}^n) - f(U_{i,j}^n))\Delta x + (g(U_{i+1,j}^n) - g(U_{i,j}^n))(y_{i+1,j} - y_{i,j})}{\Delta x^2 + (y_{i+1,j} - y_{i,j})^2},$$

while for the vertical edges the LF approximation is the same as for a rectangular grid, namely,

$$U_{i,j+1/2}^{n+1/4} = \frac{1}{2}\left(U_{i,j+1}^n + U_{i,j}^n\right) + \frac{\Delta t}{4}\frac{g(U_{i,j+1}^n) - g(U_{i,j}^n)}{y_{i,j+1} - y_{i,j}}.$$

5.3 LF Corrector

The LF corrector is same as LF predictor but with the grid shifted by $(1/2, 1/2)$, thereby interchanging the original and dual grids. For completeness we present also the formulas for the LF corrector. For the grid, see Fig. 4. We need here the area of the cell with center at the node (i, j)

$$S_{i-1/2} = 2(s_{i-1/2} + s_i)$$

(cell is denoted by its lower left corner). The LF corrector is then

$$\begin{aligned} S_{i-1/2}U_{i,j}^{n+1} = {} & s_{i-1/2}U_{i-1/2,j-1/2}^{n+1/2} + s_iU_{i+1/2,j-1/2}^{n+1/2} + s_iU_{i+1/2,j+1/2}^{n+1/2} + s_{i-1/2}U_{i-1/2,j+1/2}^{n+1/2} \\ & -\frac{\Delta t}{2}\Big[-F_{i,j-1/2}(y_{i+1/2,j-1/2} - y_{i-1/2,j-1/2}) \\ & \quad -F_{i+1/2,j}(y_{i+1/2,j+1/2} - y_{i+1/2,j-1/2}) \\ & \quad +F_{i,j+1/2}(y_{i+1/2,j+1/2} - y_{i-1/2,j+1/2}) \\ & \quad +F_{i-1/2,j}(y_{i-1/2,j+1/2} - y_{i-1/2,j-1/2})\Big] \\ & +\frac{\Delta t\Delta x}{2}\left[G_{i,j+1/2} - G_{i,j-1/2}\right], \end{aligned}$$

where the fluxes F, G are given by

$$F_{kl} = f(U_{kl}^{n+3/4}), G_{kl} = g(U_{kl}^{n+3/4})$$

with

$$\begin{aligned} U_{i,j+1/2}^{n+3/4} = {} & \frac{1}{2}\left(U_{i-1/2,j+1/2}^{n+1/2} + U_{i+1/2,j+1/2}^{n+1/2}\right) + \frac{\Delta t}{4}\left[\frac{(f(U_{i+1/2,j+1/2}^{n+1/2}) - f(U_{i-1/2,j+1/2}^{n+1/2}))\Delta x}{\Delta x^2 + (y_{i+1/2,j+1/2} - y_{i-1/2,j+1/2})^2}\right. \\ & \left. + \frac{(g(U_{i+1/2,j+1/2}^{n+1/2}) - g(U_{i-1/2,j+1/2}^{n+1/2}))(y_{i+1/2,j+1/2} - y_{i-1/2,j+1/2})}{\Delta x^2 + (y_{i+1/2,j+1/2} - y_{i-1/2,j+1/2})^2}\right] \\ U_{i+1/2,j}^{n+3/4} = {} & \frac{1}{2}\left(U_{i+1/2,j+1/2}^{n+1/2} + U_{i+1/2,j-1/2}^{n+1/2}\right) + \frac{\Delta t}{4}\frac{g(U_{i+1/2,j+1/2}^{n+1/2}) - g(U_{i+1/2,j-1/2}^{n+1/2})}{y_{i+1/2,j+1/2} - y_{i+1/2,j-1/2}}. \end{aligned}$$

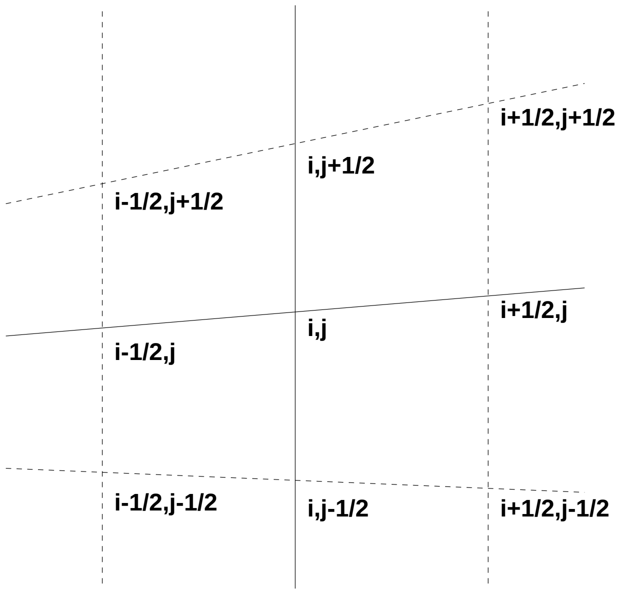

Figure 4: A part of dual grid used in CF corrector

5.4 CF corrector

A part of the dual grid which is used in the construction of CF corrector scheme is shown in Fig. 4.

The CF predictor is the same as the LF predictor (10). The CF corrector operates from the node values on the dual staggered grid at the time level $n+1/2$ to the original grid at the time level $n+1$ and is given by

$$U_{i,j}^{n+1} \equiv U_{i,j}^{n} + \frac{\Delta t}{A}\int\int (f_x + g_y)dxdy.$$

Using (9), in this case the equations are

$$\begin{aligned} U_{i,j}^{n+1} &= U_{i,j}^{n} + \frac{\Delta t}{2S_{i-1/2}}\Big[\Big(f\left(U_{i+1/2,j-1/2}^{n+1/2}\right) - f\left(U_{i-1/2,j+1/2}^{n+1/2}\right)\Big)(y_{i+1/2,j+1/2} - y_{i-1/2,j-1/2}) \\ &\quad + \Big(f\left(U_{i+1/2,j+1/2}^{n+1/2}\right) - f\left(U_{i-1/2,j-1/2}^{n+1/2}\right)\Big)(y_{i-1/2,j+1/2} - y_{i+1/2,j-1/2}) \\ &\quad + \Delta x\Big(g\left(U_{i+1/2,j+1/2}^{n+1/2}\right) + g\left(U_{i-1/2,j+1/2}^{n+1/2}\right) \\ &\qquad - g\left(U_{i+1/2,j-1/2}^{n+1/2}\right) - g\left(U_{i-1/2,j-1/2}^{n+1/2}\right)\Big)\Big]. \end{aligned}$$

This CF scheme appears to be second order accurate on smooth grids, like the grids used in section 6.3. However it is only first order accurate on the rough grids. The accuracy checking has been done by a numerical convergence test with a smooth solution.

The composite schemes on the trapezoidal mesh are constructed from the CF and LF schemes in the same way as in previous cases.

6 Numerical Results

In this section we present several test examples showing how the composite schemes work for the 2D shallow water equations.

6.1 Circular Dam Break Problem

This problem was first solved in [2], then also in [11]. The solution area is a square $(0, 50m) \times (0, 50m)$. In the center of the square is a cylindrical dam with radius 11 m. The initial water level is 10 m inside the dam and 1 m outside the dam and water is initially at rest. Suddenly the cylindrical wall making the dam disappears and time evolution of water movement is calculated. The contour plot of water height at time 0.69 s is in Fig. 5. For better insight we present also the surface plot in Fig. 6. Calculation is done on the grid of 50×50 cells as in [2] by the CFLF4 method. The plots show that the circular symmetry is preserved very well. The results agree with [2, 11].

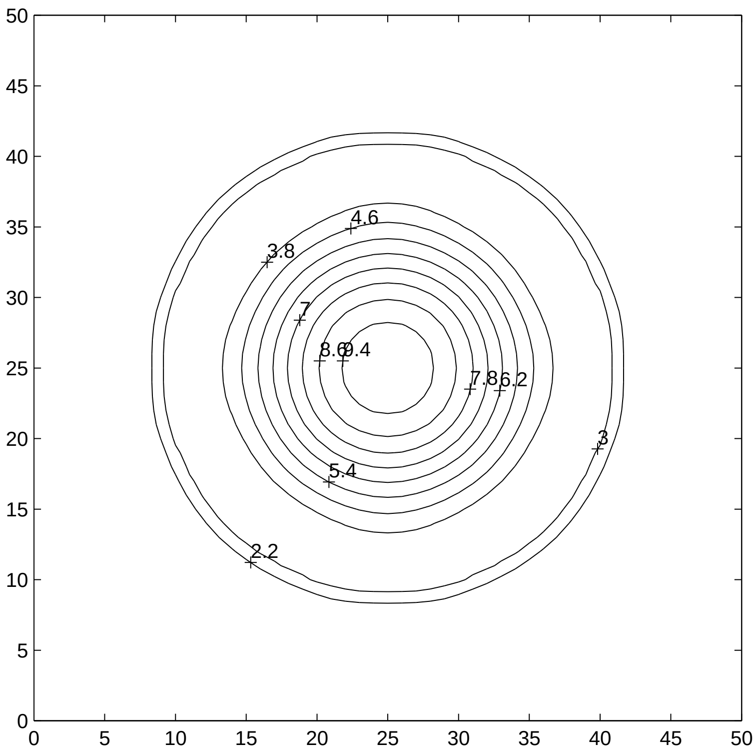

Figure 5: Contour plot of water height for the circular dam break problem

6.2 Shock Focusing Problem

The shock focusing problem originates in [16] and has been solved also in [9]. The square domain $(-1.5, 1.5) \times (-1.5, 1.5)$ has again in the center the circular wall of the radius 0.35. The initial height is 0.1 inside the wall and 1 outside. Initially the system is at rest. After removing the wall the circular shock is moving inwards, passes though the singularity and then the circular shock is

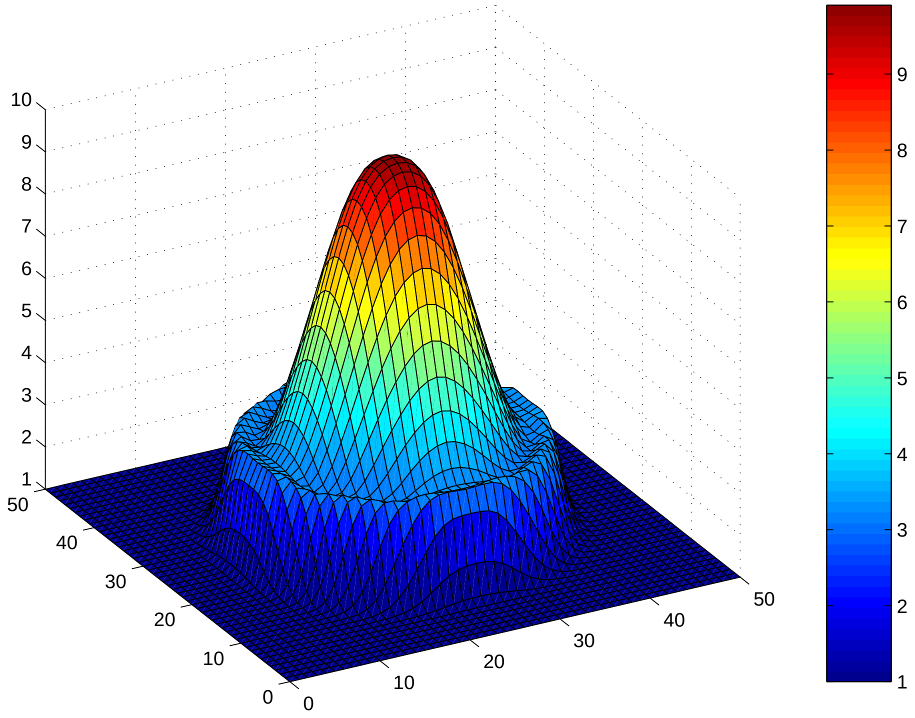

Figure 6: Surface plot of water height for the circular dam break problem

expanding outwards. The expanding shock at time $t = 1$ is plotted in Fig. 7 as a countour plot. In this calculation we use dimensionless $g = 1$. We use the mesh with 160×160 points as in [9]. Again circular symmetry is preserved very well.

For comparison we have also computed the solution of the 1D circularly symmetric shallow water equations

$$
\begin{aligned}
h_t + M_r &= 0 \\
M_t + \left(\frac{M^2}{h} + \frac{1}{2}g\frac{h^2}{r}\right)_r - \frac{1}{2}g\frac{h^2}{r^2} &= 0,
\end{aligned}
$$

where a conserved momentum M is given by $M = hu$, by the LWLF4 method on (0,1.5) with 5 000 points. This solution is a good approximation of the exact solution. In Fig. 8 we compare x and diagonal strips of the 2D CFLF2 solution with the 1D radial symmetric solution. Both height (uper plot) and velocity are plotted. Even for this hard problem shocks are resolved quite well, x and diagonal strips are almost same. Recall that CFLF2 is only a first order method.

We have also tried the second order CFCW2 composite scheme. The comparison of x and diagonal strips for height and velocity with the 1D radial solution is in Fig. 9. The solution is resolved a bit better in continuum areas. Symmetry is preserved again very well. Note that in [9] two second order methods had troubles with velocity differences of x and diagonal strips around the origin.

6.3 Supercritical Channel Flows

These supercritical (Froude number $F_R = u/\sqrt{gh} > 1$) flow test cases include flows through the channel with wall constrictions. Their solution is a steady state flow with hydraulic and negative

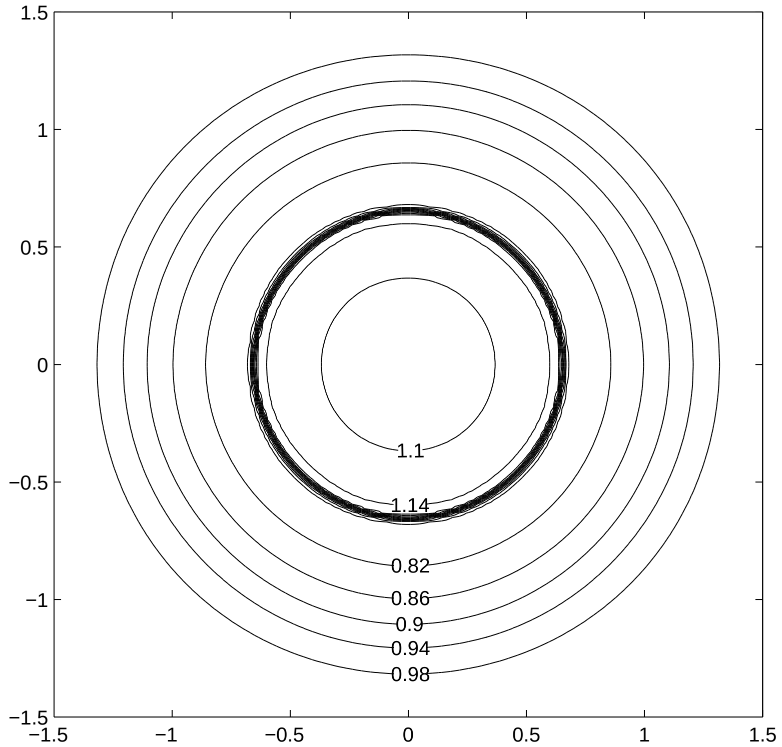

Figure 7: Contour plot of height for the shock focusing problem

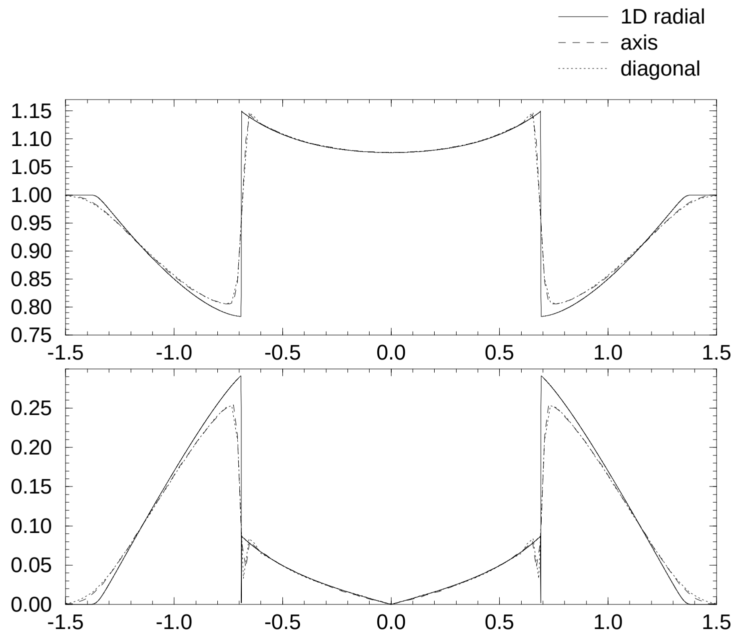

Figure 8: Axis and diagonal profile of height and velocity for the shock focusing problem by CFLF2 scheme. 1D radial symmetric solution is a good approximation of exact solution.

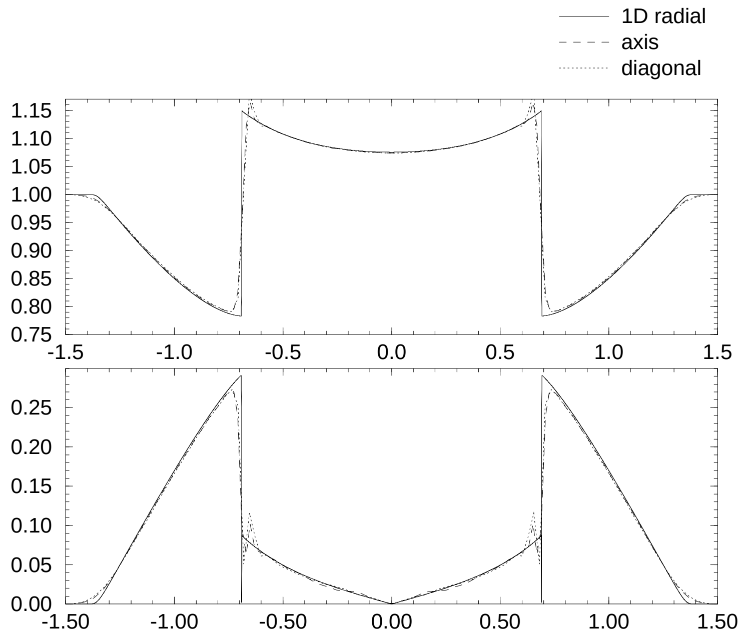

Figure 9: Axis and diagonal profile of height and velocity for the shock focusing problem by CFCW2 scheme. The 1D radially symmetric solution is a good approximation of the exact solution.

jumps. Wall constriction is given by the angle α.

6.3.1 Oblique Hydraulic Jump

The first problem is the wall constriction by the angle $\alpha = 8.95°$. The initial and inflow conditions are the height $h_0 = 1m$ and velocity $u_0 = 8.57m/s$. The geometry of the problem with the 41×31 mesh is given in Fig. 10. On the inflow left hand side we have used inflow, fixed boundary conditions, on the upper and right outflow sides we have used free boundary conditions and on the lower wall side slip (free height and zero normal velocity) boundary conditions. The contour plot of the steady state solution is in Fig. 11. For this problem the analytical solution can be computed. The shock angle $\beta = 29.72°$ from the numerical solution agrees well with the analytical result $\beta = 30°$ [2]. Also the numerical height and velocity $h_2 = 1.5005, |\mathbf{u}_2| = 7.9787$ agree well with the analytical prediction $h_2 = 1.5, |\mathbf{u}_2| = 7.9556$ [2].

The second problem is the wall constriction given by the angle $\alpha = 15°$. The initial and inflow conditions are height $h_0 = 1$ and Froude number $F_r = 3$. The geometry of the problem with the 55×37 mesh is given in Fig. 12. The boundary conditions were same as in the previous test. The contour plot of the steady state solution is in Fig. 13. The shock angle $\beta = 34.14°$ from the numerical solution agrees well with the analytical result $\beta = 34.36°$ [6].

6.3.2 Symmetric Channel Constriction

In this example the channel wall is symetrically constricted from both sides with angle $\alpha = 5°$. The initial and inflow conditions are the height $h_0 = 1$ and Froude number $F_r = 2.5$. The geometry of the problem with the 61×27 mesh is given in Fig. 14. The contour plot of the steady state solution is in Fig. 15 and shows the cross-wave pattern. For more insight we present also the

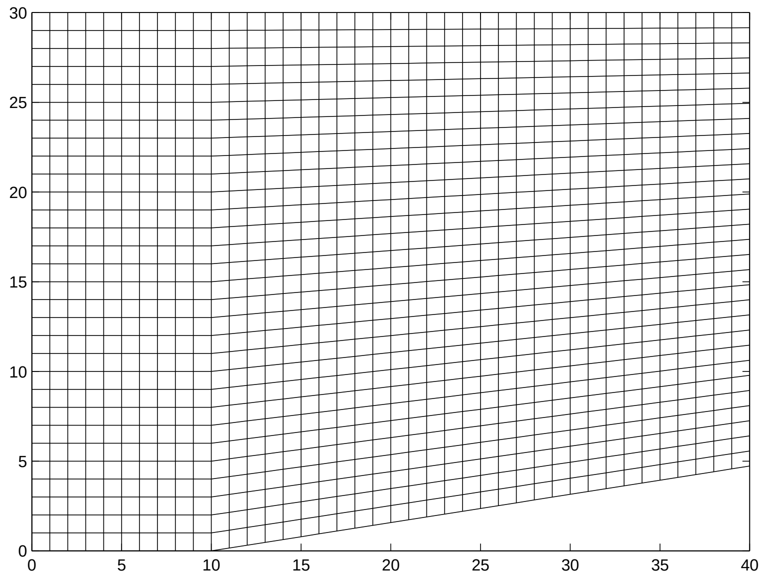

Figure 10: Geometry and mesh for the oblique hydraulic jump problem with $\alpha = 8.95°$.

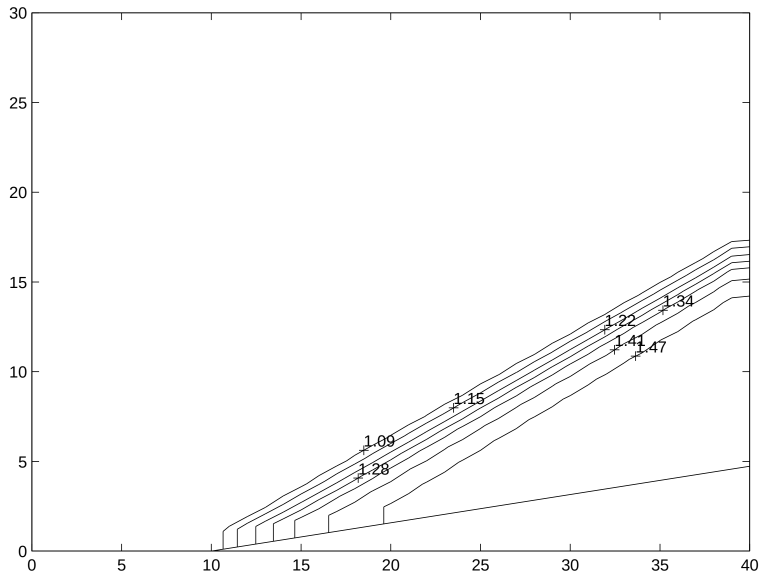

Figure 11: Contour plot of the oblique hydraulic jump problem with $\alpha = 8.95°$.

surface plot in Fig. 16. In this case again we can compare numerical results with analytical ones [6]. Numerical values of the heights $h_2 = 1.249, h_3 = 1.527$ of the first and second plateau agree well with analytical results $h_2 = 1.254, h_3 = 1.55$ [6].

6.3.3 Symmetric Channel with Variable Width

In the last example the channel wall is symetrically constricted from both sides with angle $\alpha = 15°$ and after constriction follows again a straight narrower channel. The geometry of the problem

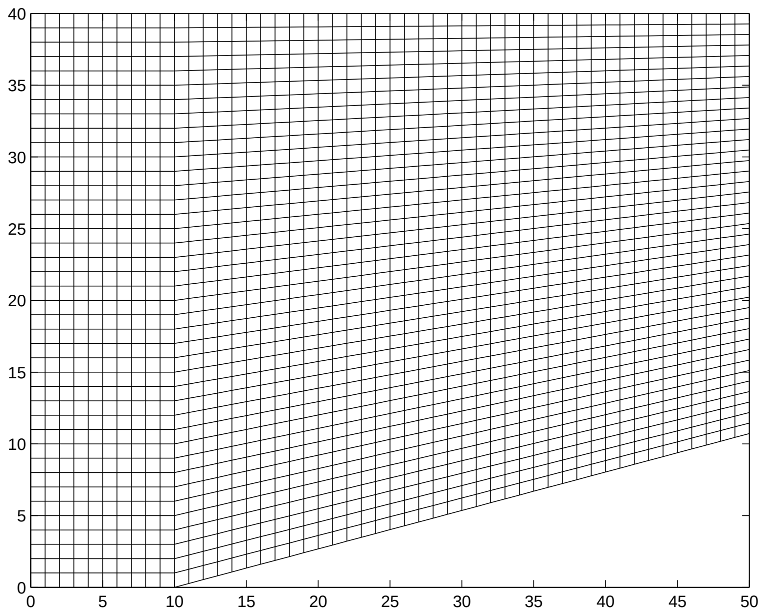

Figure 12: Geometry and mesh for the oblique hydraulic jump problem with $\alpha = 15°$.

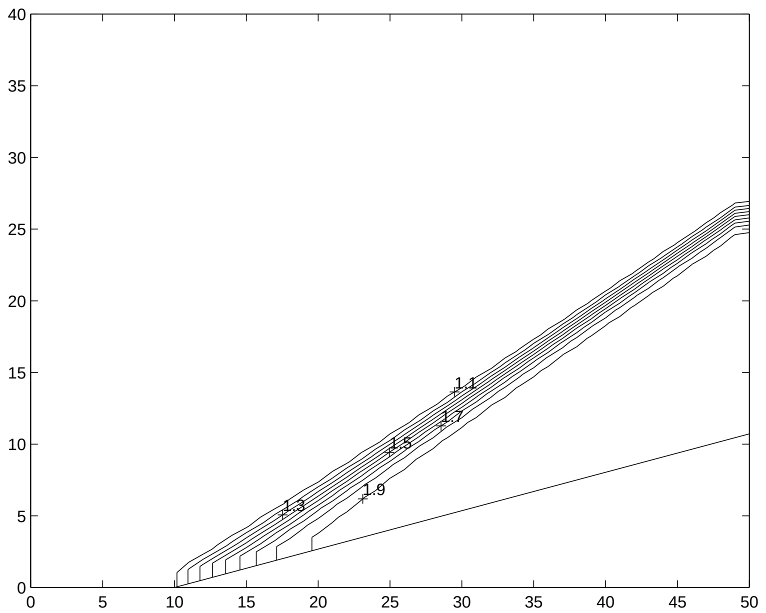

Figure 13: Contour plot of the oblique hydraulic jump problem with $\alpha = 15°$.

with the 73×33 mesh is given in Fig. 17. The initial and inflow conditions are the height $h_0 = 1$ and Froude number $F_r = 2.5$. The contour plot of the steady state solution is in Fig. 18. For more insight we present also the surface plot in Fig. 19. The results show again a cross-wave pattern which inlcudes not only hydraulic jumps as in previous examples, but also negative jumps which are caused by the presence of concave corners. On the relatively rough grid the shocks are again resolved quite nicely.

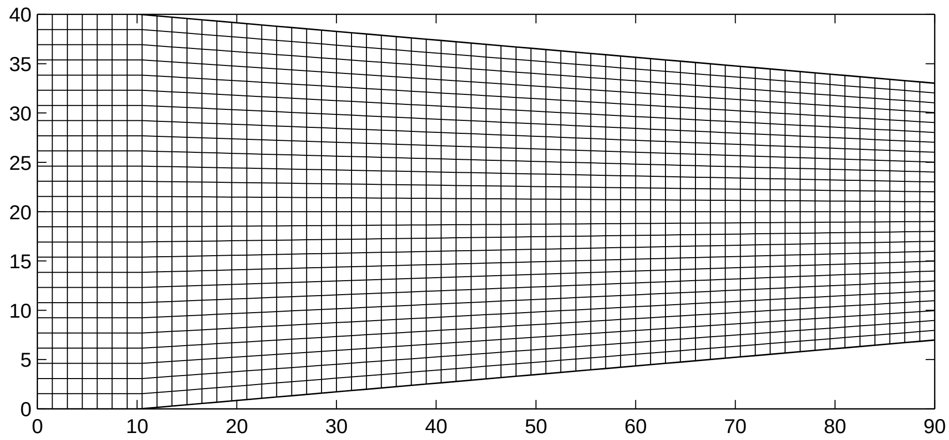

Figure 14: Geometry and mesh for the symmetric channel constriction problem

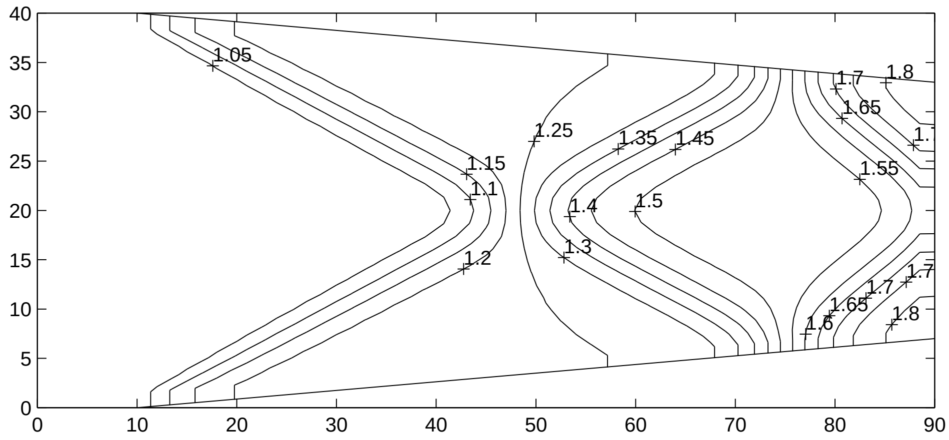

Figure 15: Contour plot for the symmetric channel constriction problem

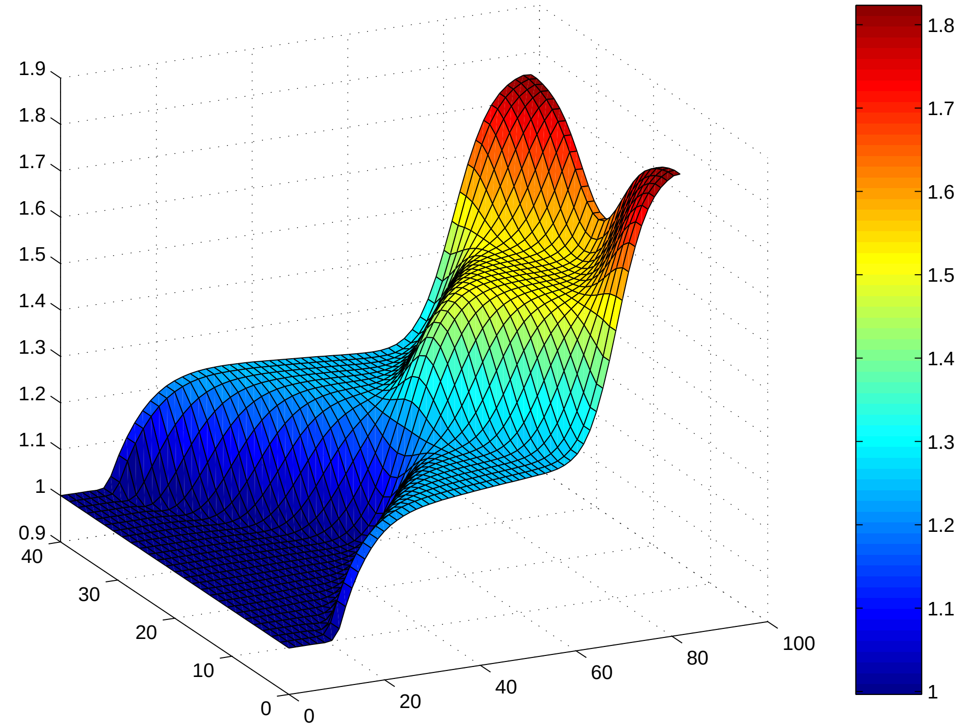

Figure 16: Surface plot for the symmetric channel constriction problem

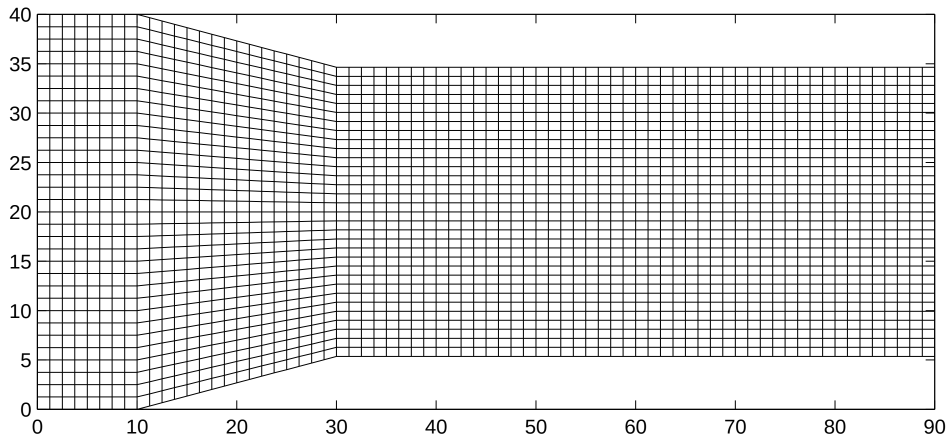

Figure 17: Geometry and mesh for the symmetric channel with variable width problem

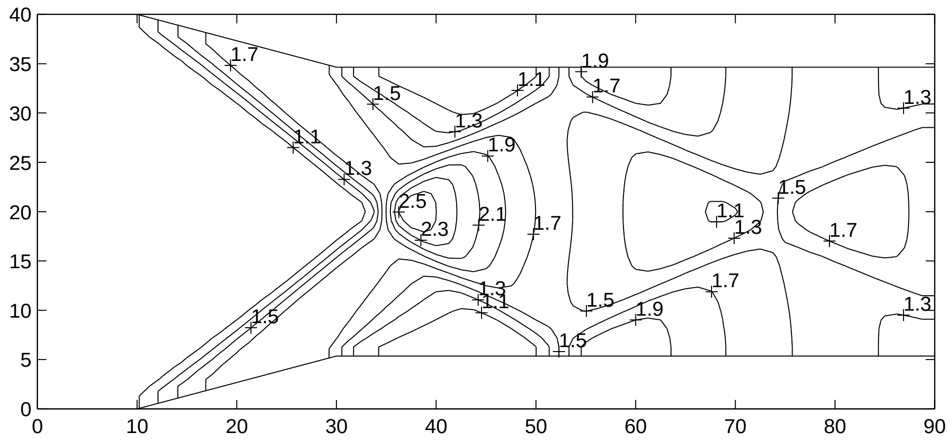

Figure 18: Contour plot for the symmetric channel with variable width problem

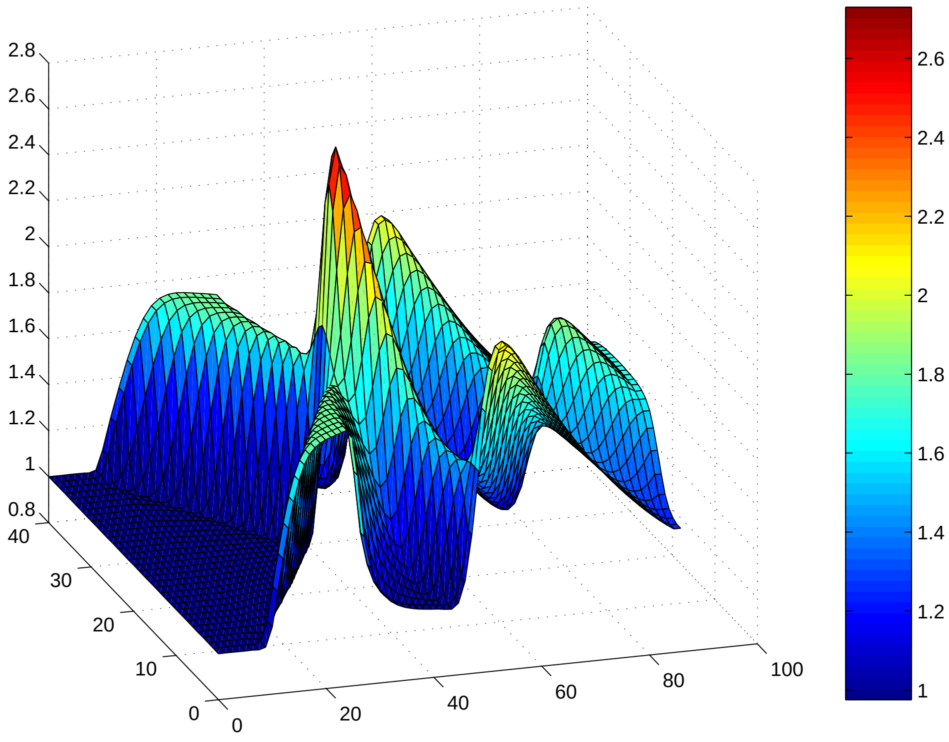

Figure 19: Surface plot for the symmetric channel with variable width problem

7 Conclusion

The composite Lax-Wendroff Lax-Friedrichs schemes have been generalized to trapezoidal meshes and applied to 2D shallow water flows in a constricted channel. This composite and the Lax-Wendroff WENO composite have been applied to the dam breaking problem. The effectiveness and robustness of this approach has been shown on several test examples. Although we have not done any speed comparison with other methods we believe that these simple schemes result in a rather fast numerical algorithm.

Acknowledgements

Both authors were partially supported by the CHAMMP program of the US Department of Energy. R. Liska was supported in part by the National Science Foundation grant CCR-9531828 and Czech Ministry of Education grant Kontakt ME 050 (1997).

R. Liska would like to thank the Institute for Geophysics and Planetary Physics of the Los Alamos National Laboratory for hosting his visit at Los Alamos.

References

[1] R. Liska and B. Wendroff. Composite schemes for conservation laws. Technical Report LA-UR 96-3589, LANL, Los Alamos, 1996. SIAM J. Numer. Anal., 1997, to appear.

[2] F. Alcrudo and P. Garcia-Navarro. A high-resolution godunov-type scheme in finite volumes for the 2d shallow-water equations. *Int. J. for Numerical Methods in Fluids*, 16:489–505, 1993.

[3] P. Glaister. Flux difference splitting for open-channel flows. *Int. J. for Numerical Methods in Fluids*, 16:629–654, 1993.

[4] B.T. Nadiga. An adaptive discrete-velocity model for the shallow water equations. *J. Comp. Phys.*, 121:271–280, 1995.

[5] B.T. Nadiga, L.G. Margolin, and P.K. Smolarkiewicz. Semi-lagrangian shallow water modeling on the cm-5. In A. Ecer, J. Periaux, N. Satofuka, and S. Taylor, editors, *Parallel Computational Fluid Dynamics: Implementations and Results Using Parallel Computers, Proceedings of the Parallel CFD'95 Conference, Pasadena, CA, U.S.A., 26-29 June, 1995*, pages 529–536, Amsterdam, 1996. Elsevier.

[6] O.C. Zienkiewicz and P. Ortiz. A split-characteristic based finite element model for the shalllow water equations. *Int. J. for Numerical Methods in Fluids*, 20:1061–1080, 1995.

[7] D. Ambrosi. Approximation of shallow water equations by roe's riemann solver. *Int. J. for Numerical Methods in Fluids*, 20:157–168, 1995.

[8] S.W. Bova and G.F. Carey. An entropy variable formulation ans applications for the two-dimensional shallow water equations. *Int. J. for Numerical Methods in Fluids*, 23:29–46, 1996.

[9] A.T. Morel, M. Fey, and J. Maurer. Multidimensional high order method of transport for the shallow water equations. In J.A. Desideri, C. Hirsch, P. Le Tallec, M. Pandolfi, and J. Periaux, editors, *Computational Fluid Dynamics '96, Proceedings of the Third ECCOMAS Computational Fluid Dynamics Conference, 9-13 Sept 1996, Paris*, pages 993–999, New York, 1996. J. Wiley.

[10] R.A. Walters and E.J. Barragy. Comparison of h and p finite element approximations of the shallow water equations. *Int. J. for Numerical Methods in Fluids*, 24:61–79, 1997.

[11] K. Anastasiou and C.T. Chan. Solution of the 2d shallow water equations using the finite volume method on unstructured triangular meshes. *Int. J. for Numerical Methods in Fluids*, 24:1225–1245, 1997.

[12] S. Chippada, C.N. Dawson, M.L. Martinez, and M.F. Wheeler. A godunov-type finite volume method for the system of shallow water. Technical Report 96-57, TICAM, University of Texas, Austin, 1997.

[13] D. D. Houghton and A. Kasahara. Nonlinear shallow fluid flow over an isolated ridge. *Comm. Pure Appl. Math.*, 21:1–23, 1968.

[14] T. Boukadida and A.-Y. LeRoux. A new version of the two-dimensional Lax-Friedrichs scheme. *Math. Comp.*, 63:541–553, 1994.

[15] Guan-Shan Jiang and Chi-Wang Shu. Efficient implementation of weighted eno schemes. *J. Comp. Phys.*, 126:202–228, 1996.

[16] S.J. Billet. *A Class of Upwind Methods for Conservation Laws.* PhD thesis, Carnfield University, 1994.